Published in Journal of Colloid and Interface Science, issue 293, 151-157, 2006
which should be used for any reference to this work

Filling kinetics of liquids in nanochannels as narrow as 27 nm by capillary force

Anpan Han, Giampietro Mondin, Nicole G. Hegelbach, Nicolaas F. de Rooij, Urs Staufer *

Institute of Microtechnology, University of Neuchâtel, Rue Jaquet-Droz 1/C.P. 3, CH-2007 Neuchâtel, Switzerland

Abstract

We report the filling kinetics of different liquids in nanofabricated capillaries with rectangular cross-section by capillary force. Three sets of channels with different geometry were employed for the experiments. The smallest dimension of the channel cross-section was respectively 27, 50, and 73 nm. Ethanol, isopropanol, water and binary mixtures of ethanol and water spontaneously filled nanochannels with inner walls exposing silanol groups. For all the liquids the position of the moving liquid meniscus was observed to be proportional to the square root of time, which is in accordance with the classical Washburn kinetics. The velocity of the meniscus decreased both with the dimension of the channel and the ratio between the surface tension and the viscosity. In the case of water, air-bubbles were spontaneously trapped as channels were filled. For a binary mixture of 40% ethanol and water, no trapping of air was observed anymore. The filling rate was higher than expected, which also corresponds to the dynamic contact angle for the mixture being lower than that of pure ethanol. Nanochannels and porous materials share many physicochemical properties, e.g., the comparable pores size and extremely high surface to volume ratio. These similarities suggest that our nanochannels could be used as an idealized model to study mass transport mechanisms in systems where surface phenomena dominate.

Keywords: Ethanol; Isopropanol; Water; Ethanol–water mixture; Capillary force; Wetting; Filling kinetics; Nanochannels; Porous materials

1. Introduction

For bionanotechnology, studying single molecules, and physicochemical phenomena of liquids in the nanometer scale nanofluidic devices provide a novel tool [1–6]. Downsizing of fluidic systems is attractive for fundamental studies as well as biosensing [7–9]. For example, nanometer-sized entropic traps were used to separate long, genomic DNA [2,3]. Nanochannels combined with near-field microscopy could be used to locate genes [10]. Furthermore, by using nanofluidic systems extremely small measurement volumes, which provide enhanced detection of enzymatic reactions, could be obtained [5]. Novel and interesting physicochemical and thermodynamic phenomena associated with liquids confined in nanofluidic systems such as double-layer overlap [11], negative pressure induced by capillary force [6], and ion enrichment–depletion effects [12], have been reported.

A less studied physicochemical effect, which is inherent for all nanofluidic devices, is the spontaneous filling by capillary force. The kinetics of filling by capillary force was first reported by Washburn in 1921 [13]. The position of the moving liquid menisci during filling was found to be proportional to the square root of the filling time. Many reported nanofluidic systems fabricated by micro- and nanolithography have rectangular cross-section and channel walls are often composed of silicon nitride and silicon dioxide [6,14,15]. The filling kinetics of channels with non-cylindrical cross-section was also studied [16–19]. To our knowledge, the smallest capillary used for kinetic studies weas pulled quartz capillaries with inner diameter of 80 nm [20]. In this article we report how different liquids fill silicon nitride/dioxide nanochannels, which inner surface

* Corresponding author. Fax: +41 (0) 32 7250711.
E-mail address: urs.staufer@unine.ch (U. Staufer).

chemistry mainly consists of hydrophilic silanol groups, by capillary force. The filling kinetics of wetting liquids followed the classical Washburn kinetics. Filling studies using water and binary mixtures of ethanol and water show phenomena similar to that observed in porous material such as trapping of the non-wetting phase.

2. Theory

A simple model for the filling kinetics by capillary force in capillaries with rectangular cross-section is used for this study. For a capillary with circular cross-section and inner radius of r, the capillary pressure is given as $p = 2\gamma\cos\theta_d/r$, where γ and θ_d are the surface tension of the liquid and the dynamic contact angle, respectively. According to White [21], this equation can be used to calculate the capillary pressure in capillaries with rectangular cross-section if r is substituted with the hydraulic radius, $r_H = A/s = r/2$, where A is the cross-section area and s is the wetted perimeter. For a rectangular channel $r_H = A/s = wd/2(w+d)$, where w is the width and d is the depth (Figs. 1 and 2). For our nanochannels, d is small compared to w, and we approximated $r_H \approx d/2$. Hence, the capillary pressure in a rectangular channel is $p = 2\gamma\cos\theta_d/d$. We neglect the effects of the static pressure (<1 mbar), which is justified since the capillary pressure in our nanochannels was calculated to be above 3 bar. The dynamic filling of a capillary with circular cross-section by capillary pressure, assuming the non-slip condition, is given by the Washburn equation [13]. The meniscus velocity, v, also referred as the filling rate is given by

$$v = \frac{r\gamma\cos\theta_d}{4\eta}\frac{1}{l}, \tag{1}$$

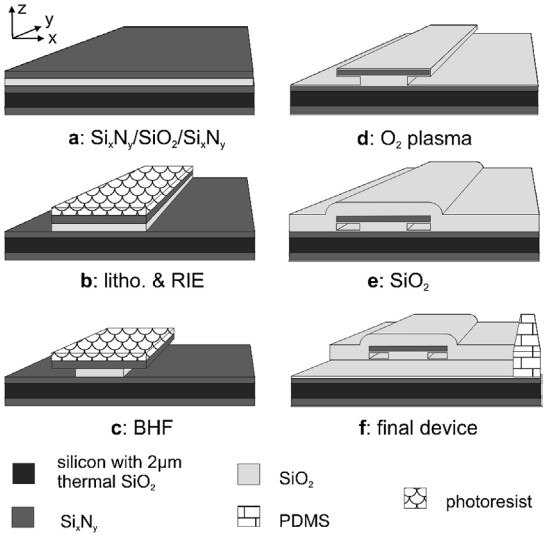

Fig. 1. Pseudo 3-D and cross-section representation of the fabrication process of a pair of nanochannels. Details are given in Section 3. Note that the dimensions of the illustration are neither scale nor proportions.

where l is the distance between the capillary meniscus and the capillary inlet, and η is the viscosity of the liquid. To obtain the meniscus velocity for a capillary with rectangular cross-section, we substituted the radius with the hydraulic radius, $r = 2r_H \approx d$,

$$v \approx \frac{d\gamma\cos\theta_d}{4\eta}\frac{1}{l} = \frac{D}{2l}, \tag{2}$$

$$D = \frac{d\gamma\cos\theta_d}{2\eta}. \tag{3}$$

The meniscus velocity is higher for larger surface tension to viscosity ratios and channel depth. Integrating the velocity with respect to time we get

$$l = \sqrt{\frac{d\gamma\cos\theta_d}{2\eta}}\sqrt{t} = \sqrt{D}\sqrt{t}. \tag{4}$$

The position of the meniscus relates with time as $l \sim t^{1/2}$ which is universal for conduits with arbitrary shape, including capillaries with rectangular cross-section [17]. The parameter D, which is independent of time and the meniscus

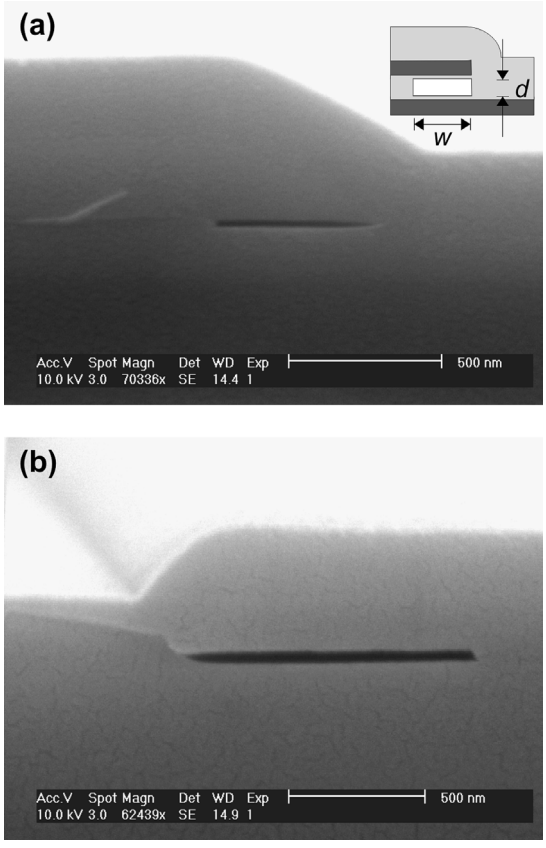

Fig. 2. Scanning electron microscopy (SEM) images of cross-sections through nanochannels fabricated by partial etching of a sacrificial layer. The figure inset in (a) corresponds to a zoom in Fig. 1e, where d is the channel depth and w is the width. Channel depth and width were measured by SEM. The black and thin "bars" about 500 nm long (a) and 900 nm long (b) are the inner cavities of the capillary, and the gray area on the picture is the wall material. The channels in (a) and (b) are respectively 27 and 50 nm deep.

position, can be determined by plotting l versus $t^{1/2}$ values. The $l \sim t^{1/2}$ scaling law originates from the capillary pressure which pulls the liquid into the channel, and which remains constant, while the flow resistance increases linearly irrespectively of the geometry of the channel cross-section. Other parameters, such as the degree of roundness of the corners of rectangular channels [17,19], the layered structure of the channel walls [22,23], and the time dependency of the dynamic contact angle [24] that influence the filling rate are not included in Eq. (2). How these issues influence the filling kinetics are going to be presented in the discussions.

3. Materials and methods

3.1. Microfabrication process of nanochannels

The nanochannel fabrication process is based on partial etching of a sacrificial layer [25]. The fabrication process only requires established micromachining techniques and does not require any nanolithography. The starting substrates were 525-µm-thick, 100-mm-diameter ⟨100⟩ silicon (Si) wafers polished on one side. The Si wafer was cleaned in a mixture of H_2SO_4 and peroxide ($(NH_4)_2S_2O_8$) at 120 °C for 10 min, followed by buffered HF (BHF; NH_4F:HF = 7:1) for 1 min, and finally in 70% HNO_3 at 115 °C for 10 min. The wafers were rinsed in doubly deionized (DI) water between the acid treatments. A layer of 2-µm-thick thermal silicon dioxide was grown. A sandwich of silicon nitride (300 nm) deposited by low-pressure chemical vapor deposition (Si_xN_y) and silicon dioxide deposited by chemical vapor deposition (SiO_2) was deposited (Fig. 1a). The depth of the nanochannels depends on the thickness of the SiO_2 layer. Process parameters for Si_xN_y deposition: temperature: 800 °C, gases: SiH_2Cl_2 and NH_3, pressure 200 mTorr; for SiO_2 deposition: temperature: 400 °C, gases: 2% SiH_4 in N_2, and O_2, pressure: atmospheric. The fabrication required two photolithography processes; the wafers were dehydrated at 200 °C for 30 min and subjected to a silanization treatment with hexamethyldisilazane. A layer of 1.8-µm-thick positive photoresist was spin-coated onto the Si wafer and prebaked for 1 min at 100 °C on a hot plate. A chromium mask with the channel features was aligned to the Si wafer. During the first photolithography, the mask patterns were transferred to the resist by exposure with UV, followed by development. After development (1 min) the photoresist was postbaked for 30 min at 125 °C in an oven. The photoresist served as a mask during the following reactive ion etching (RIE) process where the patterns were transferred into the wafer. Etching was stopped on the second layer of Si_xN_y (Fig. 1b). The sacrificial SiO_2 layer was partially under etched by BHF followed by rinsing using DI water (Fig. 1c). The width of the nanochannels was determined by the timed etch (about 200 nm/min) of the sacrificial layer. The remaining photoresist was removed by oxygen plasma. Before the encapsulation of the nanochannels, the silicon nitride was treated with oxygen plasma (Tepla 132 from PVA Tepla, Feldkirchen, Germany. Parameters: RF power 1000 W, pressure 0.73 mbar, 100 °C, 60 min) to create a surface composed mainly of silicon dioxide [26,27]. The inner surface of our nanochannels consisted of a few monolayers of silicon dioxide exposing silanol groups (Fig. 1d). To seal the channels, a fresh layer of SiO_2 (400 nm) was deposited (Fig. 1e). A second photolithography and RIE process were used to pattern the access openings to the nanochannels. A second oxygen plasma process was used to remove photoresist and create a thin layer of silicon dioxide on the wafer surface. Polydimethylsiloxane (PDMS) O-rings were prepared [28] and sealed reversibly to the access openings to serve as liquid reservoirs (Fig. 1f). Fig. 2 shows a cross-section of the fabricated nanochannels.

3.2. Experimental procedure of the filling kinetic studies

Isopropanol (VLSI grade from Rockwood, Avenches, Switzerland), ethanol (analytical grade from VWR, Le Lignon, Switzerland), mixtures of ethanol and deionized water of clean room quality (resistivity >10 MΩ/cm) and Tris (Fluka, Buchs, Switzerland) buffers spontaneously filled array of channels by capillary force. We observed the horizontally positioned nanochannel arrays using a stereomicroscope (MZ8 from Leica) with ring-illumination. We pipetted a few micromilliliters of a liquid into the PDMS reservoir located on one of the two access openings of a nanochannel array. As the array of nanochannels filled, we were able to see a change in color and contrast because of the difference between the refractive index of air in the vacant channels and the refractive index of the liquid (Fig. 3). Pictures and real-time movies were taken through a digital camera (CoolPix 5400 from Nikon, 5.1 million pixels, resolution:

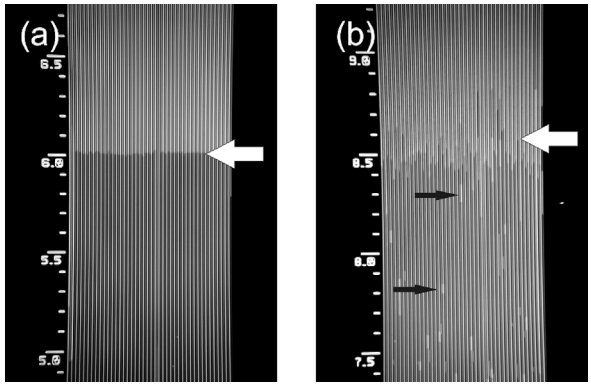

Fig. 3. Optical microscope image showing the filling of channel arrays. Each array consists of 40 pairs (Fig. 1), a total of 80 parallel nanochannels. Each channel is 900 nm wide, 50 nm deep and 15 mm long. The position of the meniscus, l, could be read from the integrated scale (8.5 indicate $l = 8.5$ mm, each minor division is 100 µm). (a) A channel array is filled with isopropanol. The thick white arrow indicates the meniscus position. The darker area below the white arrow is filled and the brighter area is empty. A few channels were not filled, e.g., middle and left. (b) Water was introduced into the channel array and bubbles were trapped during filling (thin black arrows).

2592 × 1944 pixels, 24 bit color) mounted on the stereomicroscope. Computer software Pinnacle Studio, Ver. 8.12.7.0, from Pinnacle Systems and Corel Draw 11 from Corel was respectively used for video and image analysis. For the case of the 27-nm-deep nanochannels it was necessary to digitally enhance the contrast to determine the position of the meniscus. By reviewing the real-time movies the position of the meniscus could be read from an integrated scale beside the nanochannel array, and the associated time could be read from the computer software. For ethanol, 40% ethanol, and isopropanol the position of the common meniscus was clearly defined (Fig. 3a). It was more difficult to evaluate the common meniscus for water since there was not a uniform filling of the channel arrays (Fig. 3b). Time was set to 0 s as the droplet of liquid entered the PDMS reservoir. The $(t^{1/2}, l)$ values were read and plotted.

3.3. Scanning electron and fluorescence microscopies

For fluorescence microscopy the channels were filled with 10 mM rhodamine B (Sigma, Buchs, Switzerland) dissolved in ethanol, or 10 mM fluorescein (Fluka, Buchs, Switzerland) in 10 mM Tris buffer, pH 7.2. The fluorescence signal in the nanochannels was imaged with a cooled CCD camera (CF 8/4 DXC from Kappa, Gleichen, Germany) mounted on an inverted fluorescence microscope with integrated filter sets (Axiovert S100 from Zeiss).

The depth and width of nanochannels were measured by scanning electron microscopy (SEM). The instrument was a XL30 ESEM-FEG from Philips. Samples for SEM imaging were prepared by cleaving a part of a processed wafer, such that the cut ran across the nanochannels, exposing a cross-section of the nanochannels (Fig. 2). To decrease charging effects a thin layer of AuPd (5 nm) was sputtered onto the sample before SEM.

4. Results

The kinetics of filling is determined by the liquid, the surface properties, and the geometry of the channel. We performed two sets of experiments by changing either the liquid or the channel geometry while we kept the other parameters constant.

For the first set of experiments, we investigated the filling in channel arrays using water, ethanol, isopropanol, and a two-component ethanol and water mixtures. A channel array has 80 parallel channels and it is at least 15 mm long. The individual channels in an array are 50 nm deep and 900 nm wide. The experiments were done under ambient condition (21–25 °C) without using temperature control. During water filling experiments, bubbles spontaneously appeared inside the channels (Figs. 3 and 4). Apart from water, the variation of the meniscus position within a channel array was about 1% of the filled length. Each filling experiment was performed in a fresh channel array to avoid any contamination. The meniscus position l and the associated time were read as the channels filled (Fig. 3a). The square root of time and the associated meniscus position data were plotted, and data points were fitted using a linear function.

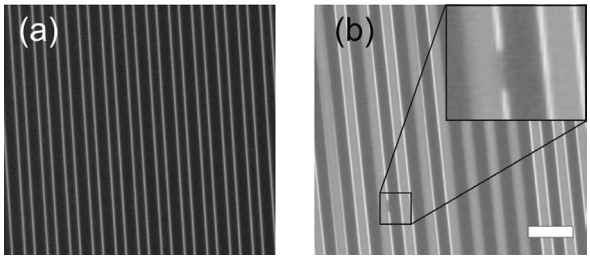

Fig. 4. Arrays of channels were filled using 10 mM rhodamine B dissolved in ethanol (a) and 10 mM fluorescein in 10 mM Tris buffer, pH 7.2 (b). Picture inset in (b) shows a magnification of a bubble trapped inside a channel. The distance between two adjacent channels (thin bright lines) is 10 µm. The scale bar is 40 µm. The pictures were taken with a cooled CCD camera using 640 ms of integration time, maximum gain and same contrast settings. The fluorescein filter set has a higher fluorescence background, and it is more sensitive to scattered light than the rhodamine set. Since the surface of the substrate is not flat because of the fabrication process (Fig. 1) the elevated surfaces are brighter than the lower surfaces.

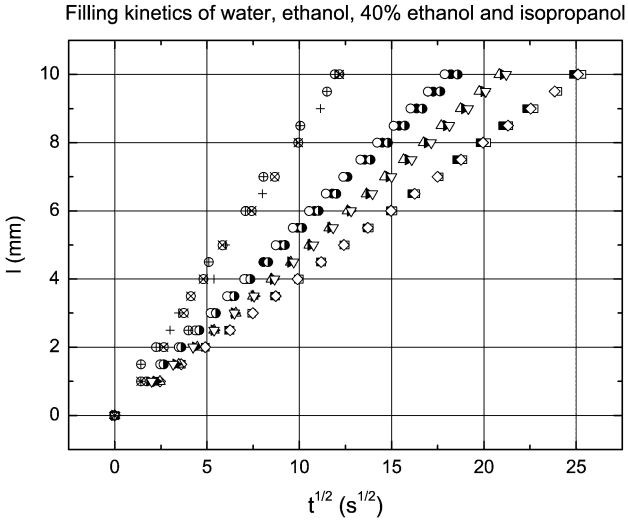

Fig. 5. Filling kinetics of water, ethanol, 40% ethanol, and isopropanol. For each liquid three channel arrays were filled. As each channel array was filled the meniscus position and associated time values were recorded. The three circular legends (○, ●, ◑) are filling experiments using ethanol, and each legend represents data from one filling experiment. The triangular (△, ►, ▽), the square legends (■, □, ◇) and the legends (+, ⊗, ⊕) correspond to filling experiments using 40% ethanol, isopropanol, and water, respectively.

For all the liquids we tested, the position of the meniscus was observed to be proportional to the square root of the time needed to fill the channel array (Fig. 5), which is in accordance with the classical Washburn kinetics. The filling rate, which is proportional to the square of the slope of the linear fit D, is higher for ethanol than isopropanol. This observation is in agreement with Eq. (2), since the ratio between surface tension and viscosity is higher for ethanol (Table 1). D was obtained for each filling experiment and the

Table 1
Summary of filling experiments in Figs. 5 and 6 and tabulated surface tension and viscosity values at 20 °C [29]

Channel depth (nm)	Channel width (nm)	Liquid	Surface tension (dyn/cm)	Viscosity (cP)	D (mm^2/s)	SD[a]	θ_d	Time to fill 10 mm[b]
50	900	Water	72.9	1.00	0.677	0.02	68	2 min 28 s
50	900	EtOH	22.8	1.20	0.300	0.002	50	5 min 33 s
50	900	Isopropanol	23.8	2.26	0.156	0.01	53	10 min 40 s
50	900	40% EtOH	32.0	2.76	0.229	0.01	38	7 min 17 s
27	500	EtOH	22.8	1.20	0.177	0.004	46	9 min 25 s
73	600	EtOH	22.8	1.20	0.402	0.02	55	4 min 9 s

D is the square of the slope obtained from linear fits of data plotted in Figs. 5 and 6.
[a] Standard deviation of D is based on three measurements performed on the same day.
[b] The time to fill channels 10 mm is the extrapolated using the fitted D values.

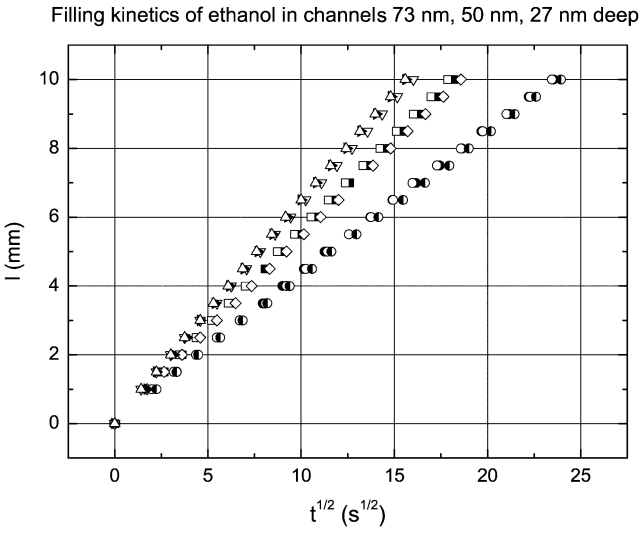

Fig. 6. Filling kinetics of ethanol in channels with different depth. For each channel depth three channel arrays were filled. As each channel array was filled the meniscus position and associated time values were recorded. The three triangular legends (△, ▶, ▽) are filling experiments using 73-nm-deep channels, and each legend represents data from one filling experiment. The rectangular (■, □, ◇) and the circular legends (○, ●, ◐) correspond to filling experiments using 50- and 27-nm-deep channels, respectively.

dynamic contact angle, θ_d, was calculated using Eq. (3) and tabulated values (Table 1). The tabulated values are valid for 20 °C [29]. Each measured D given in Table 1 is an average of three filling experiments performed on the same day. The standard variation of D for each liquid is less than 4%. For water, θ_d is 68°. For ethanol and isopropanol, θ_d is respectively 51° and 54°, and for a 40% (v/v) mixture of ethanol and water, θ_d is 38°.

In the second set of experiments, we selected ethanol as the test liquid, and studied channels of 27, 50, and 73 nm deep. The experimental conditions were the same as in the first set of experiments. Washburn kinetics was observed for all channel depths. In agreement with Eq. (1) the filling rate decreased with channel depth. Data sets of l and $t^{1/2}$ were plotted in Fig. 6, and the obtained D values are listed in Table 1. The dynamic contact angle is 46° for 27-nm-deep channels and 54° for 73-nm-deep channels.

The time needed to fill the channels using different liquids and channel depth is also given in Table 1. Depending on the particular liquid and channel depth the time to fill 10-mm-long channels tooks from 2 to 10 min.

5. Discussion

5.1. Filling kinetics of isopropanol, ethanol, and 40% ethanol in water

We quantitatively studied ethanol, isopropanol, and a two-component mixture (40% ethanol (v/v) in water) in 50-nm-deep and 900-nm-wide channels. The results we obtained were in accordance with the classical Washburn relation, the $l \sim t^{1/2}$ scaling law. This result also implied that the dynamic contact angles remained independent from time for our experiments. For many times our results were in agreement with studies in nanometer-sized quartz capillaries [20]. Sobolev et al. showed that the dynamic contact angle in nanometer-sized quartz capillaries remained independent from time for meniscus velocities larger than 5 μm/s, which is three times smaller than the lowest meniscus velocity (15.6 μm/s for ethanol in 27-nm-deep channels, $l = 10$ mm) in our studies. Since our time scale is far above the seconds, dynamic contact angle changes during the initial filling, studied using large-scale molecular dynamic simulation of pore imbibition [24], could not be observed in our experiments.

We calculated the dynamic contact angle by inserting the fitted D values, and the tabulated values for surface tension and viscosity, into Eq. (3). The values we obtained for the dynamic contact angles were all significantly larger than the equilibrium contact angles measured using a drop shape analysis system from Krüss (Germany). We could only form standing droplets using water on silicon nitride and silicon oxide surfaces. The equilibrium contact angle was about 10° for water and close to zero for the other liquids. Experiments performed by Sobolev et al. [20] showed also a huge difference between the equilibrium and dynamic contact angle. It was observed in capillaries with radii of about 50 nm, that the dynamic contact angle of water increased from 30° to 70° as the meniscus velocity increased from 0 to 8 μm/s which is slightly smaller than our smallest meniscus velocity (15.6 μm/s for ethanol in 27-nm-deep channels, $l = 10$ mm). In our experiments, θ_d was 68° for water, which

agrees well with the experimental data obtained in quartz capillaries [20]. For ethanol, θ_d was smaller than the dynamic contact angle for water which was in accordance with measurements made in glass capillaries with an inner radius of 0.295 mm [30]. The θ_d for the 40% ethanol water mixture was 38°, which was significantly smaller than θ_d for both water and ethanol. We would expect the θ_d for the mixture to be between that of ethanol and water. There are two possible explanations, either θ_d is really larger than expected, or the other parameters in the D of Eq. (2) changed. The dynamic contact angle between a fluid and a surface is dependent on the van der Waals forces. Hence, both the silicon dioxide, which is in a direct contact with the liquid, and the underlying silicon nitride influence θ_d [22,23]. However, it would be very surprising if the layered silicon oxide/nitride surface had a profound effect for the mixture compared with pure liquids. We look at Eq. (2) for other explanations. Firstly, as mentioned by Dong and Chatzis [17], the filling rate is dependent on the roundness of the corners of capillaries with rectangular cross-section. For the filling of water, ethanol, isopropanol, and 40% ethanol the same set of channels (50 nm deep) was used, and therefore the influence due to the roundness of the corners was the same for all the liquids. Hence, the geometry of the cross-section could not explain the relatively higher filling rate. The remaining parameters which influence D are the depth, the viscosity, and the surface tension. The depth of our channels, like the roundness of the corners, which only depend on the geometry, would not explain the deviation. Finally, an increase of the ratio between the surface tension and the viscosity, γ/η, would also increase the filling rate. According to tabulated viscosity and surface tension values for ethanol–water mixtures [29], 30% ethanol in water mixture has a larger γ/η value than the 40% ethanol we used to fill our nanochannels. This might hint that the ethanol content inside the nanochannels is lower than in the initial mixture, which implies a chemical selectivity of the nanochannel toward water. Porous membranes, that are used to separate mixtures of ethanol and water by pervaporation, exhibit similar properties as our nanochannels [31]. Such membranes are more permeable for water than ethanol, and of more water than ethanol entering the membrane. Also our channels and these membranes both have hydrophilic inner surface and similar pore size. The geometry of our nanochannels is uniform while pores in membranes are less well-defined. Arrays of nanochannels could hence serve as an idealized model system to achieve a better understanding of complicated transport and separation mechanisms in membrane materials.

5.2. Filling long nanochannels with water and trapping air

We also filled nanochannels using different aqueous solutions. In contrast to ethanol and isopropanol, the filling was very inhomogeneous and bubbles appeared spontaneously. With time the size of the bubbles diminished. Inhomogeneous filling and bubbles were also observed using fluorescence microscopy (Fig. 3b). The position of the common meniscus evolved with time corresponds to the Washburn kinetics, however, we do not know how individual channels are filled. Channels were also filled using other mixtures of ethanol and DI water (9%, 18%, ethanol) for which we still observed bubble formation. We were able to fill the channels uniformly without introducing bubbles using 40% ethanol, which generates a lower capillary pressure than pure water when introduced in our nanochannels.

Hibara et al. also observed inhomogeneous filling of water, but they did not observe any air trapping. This is not in contradiction to our observations, since their channels were only 100 μm long [16], and we only observed a few bubbles for every millimeter after the channels were filled (Fig. 3b). Similar trapping of the non-wetting phase (air in our case) during imbibition (injecting a wetting fluid) is a well-known phenomenon in porous media [32,33]. In the range of intermediate to high flow rates, the amount of the trapped non-wetting phase decreases with capillary pressure [33], which is in accordance to our observations. The dimensions between adjacent particles in porous media are comparable to the depth and width of our channels. Therefore, nanochannels could also prove useful as a model system for studying wetting of porous materials under this aspect.

5.3. Washburn kinetics in channels with different depth

To our knowledge, 27-nm-deep channels are the smallest channels where filling kinetics by capillary force was studied. This was only possible because of the recent advances in the innovative development of cost-effective fabrication methods of nanochannels [15,25,34–36]. The filling rate decreased with diminishing channel depth (Fig. 5), which is in accordance with Eq. (2). The $l \sim t^{1/2}$ relation was observed for channels down to about 27 nm. Other filling kinetics studies of channels with rectangular cross-section were performed with much larger channels. Yang et al. reported the marching velocity of capillary menisci in 500-nm-deep silicon nitride channels [18]. Hibara et al. reported filling kinetics in 300-nm-deep channels fabricated in fused silica [16]. Both investigated channels of rectangular cross-section and they also observed the $l \sim t^{1/2}$ relation. Sobolev et al. made kinetics studies in channels with circular cross-section using pulled quartz capillaries with diameters so small as 80 nm [20]. None of the filling studies in nanochannels including ours showed any clear signs of abrupt physicochemical changes such as phase transitions [37].

6. Conclusions

Using a novel and inexpensive technique, we fabricated nanochannels with which we performed filling kinetics studies using different liquids in capillaries down to 27 nm. The position of the moving liquid meniscus during filling was observed to be proportional to the square root of time

needed for filling, which corresponded to the classical Washburn filling kinetics. For pure liquids such as ethanol and isopropanol the experimental results agreed with the theoretical model based on filling by capillary force. For two-component ethanol–water mixtures significant deviation toward higher filling rates were observed. We conclude therefore that nanochannels may have a chemical selectivity toward water compared to ethanol. However, we cannot exclude that the deviation may also be caused by the dynamic contact angle of the mixture being smaller than that of pure ethanol or water. Moreover, we observed trapping of the non-wetting phase (air) during filling with water, which was also observed by others in porous materials. The extreme surface to area ratio of our nanochannel is comparable to pores in membrane materials. The high uniformity of the presented nanochannels could be used as an idealized model to study highly complex mass transport mechanisms in porous materials.

Acknowledgments

The authors thank the technical staff of ComLab, the joint IMT–CSEM clean room facility. The authors also thank the reviewers of the Journal of Colloid and Interface Science for suggestions and constructive critics. Anpan Han also acknowledges the Danish Research Agency for the financial support (Grant: Internationaliseringsstipendium) for his Ph.D. studies at IMT, University of Neuchâtel.

References

[1] S.R. Quake, A. Scherer, Science 290 (2000) 1536.
[2] J. Han, H.G. Craighead, Science 288 (2000) 1026.
[3] N. Kaji, Y. Tezuka, Y. Takamura, M. Ueda, T. Nishimoto, H. Nakanishi, Y. Horiike, Y. Baba, Anal. Chem. 76 (2004) 15.
[4] M.B. Stern, M.W. Geis, J.E. Curtin, J. Vac. Sci. Technol. B 15 (1997) 2887.
[5] M.J. Levene, J. Korlach, S.W. Turner, M. Foquet, H.G. Craighead, W.W. Webb, Science 299 (2003) 682.
[6] N.R. Tas, P. Mela, T. Kramer, J.W. Berenschot, A. van den Berg, Nano Lett. 3 (2003) 1537.
[7] J.L. Li, M. Gershow, D. Stein, E. Brandin, J.A. Golovchenko, Nat. Mater. (2003) 611.
[8] A. Mara, Z. Siwy, C. Trautmann, J. Wan, F. Kamme, Nano Lett. 4 (2004) 497.
[9] H. Bayley, C.R. Martin, Chem. Rev. 100 (2000) 2575.
[10] W.L. Li, J.O. Tegenfeldt, L. Chen, R.H. Austin, S.Y. Chou, P.A. Kohl, J. Krotine, J.C. Sturm, Nanotechnology 14 (2003) 578.
[11] J.M. Ramsey, J.P. Alarie, S.C. Jacobsen, N.J. Peterson, in: Y. Baba, S. Shoji, A. van den Berg (Eds.), Micro Total Analysis Systems 2002, vol. 1, Kluwer Academic, Dordrecht, 2002, p. 314.
[12] Q.S. Pu, J.S. Yun, H. Temkin, S.R. Liu, Nano Lett. 4 (2004) 1099.
[13] E.W. Washburn, Phys. Rev. 17 (1921) 273.
[14] M. Foquet, J. Korlach, W. Zipfel, W.W. Webb, H.G. Craighead, Anal. Chem. 74 (2002) 1415.
[15] H. Cao, Z.N. Yu, J. Wang, J.O. Tegenfeldt, R.H. Austin, E. Chen, W. Wu, S.Y. Chou, Appl. Phys. Lett. 81 (2002) 174.
[16] A. Hibara, T. Saito, H.B. Kim, M. Tokeshi, T. Ooi, M. Nakao, T. Kitamori, Anal. Chem. 74 (2002) 6170.
[17] M. Dong, I. Chatzis, J. Colloid Interface Sci. 172 (1995) 278.
[18] L.J. Yang, T.J. Yao, Y.C. Tai, J. Micromech. Microeng. 14 (2004) 220.
[19] T.C. Ransohoff, C.J. Radke, J. Colloid Interface Sci. 121 (1988) 392.
[20] V.D. Sobolev, N.V. Churaev, M.G. Velarde, Z.M. Zorin, J. Colloid Interface Sci. 222 (2000) 51.
[21] F.M. White, Fluid Mechanics, fourth ed., McGraw–Hill, Singapore, 1999.
[22] A.W. Adamson, A.P. Gast, Physical Chemistry of Surfaces, sixth ed., Wiley, New York, 1997.
[23] G.W. Wang, Y. Zhang, Y.P. Zhao, G.T. Yang, J. Micromech. Microeng. 14 (2004) 1119.
[24] G. Martic, F. Gentner, D. Seveno, J. De Coninck, T.D. Blake, J. Colloid Interface Sci. 270 (2004) 171.
[25] A. Han, G. Mondin, N.G. Hegelbach, N.F. de Rooij, U. Staufer, in: T. Laurell, J. Nilsson, K. Jensen, D.J. Harrison, J.P. Kutter (Eds.), Micro Total Analysis Systems 2004, vol. 1, The Royal Society of Chemistry, Malmö, Sweden, 2004, p. 309.
[26] G.P. Kennedy, S. Taylor, W. Eccleston, W.M. Arnoldbik, F. Habraken, Microelectron. Eng. 28 (1995) 141.
[27] S. Weichel, R. de Reus, S. Bouaidat, P.A. Rasmussen, O. Hansen, K. Birkelund, H. Dirac, Sens. Actuators A Phys. 82 (2000) 249.
[28] D.C. Duffy, J.C. McDonald, O.J.A. Schueller, G.M. Whitesides, Anal. Chem. 70 (1998) 4974.
[29] R.C. Weast, CRC Handbook of Chemistry and Physics, CRC, Boca Raton, 1988.
[30] A. Hamraoui, K. Thuresson, T. Nylander, V. Yaminsky, J. Colloid Interface Sci. 226 (2000) 199.
[31] X.S. Feng, R.Y.M. Huang, Ind. Eng. Chem. Res. 36 (1997) 1048.
[32] F.A.L. Dullien, Porous Media, Fluidic Transport and Pore Structure, second ed., Academic Press, New York, 1992, p. 117.
[33] M. Blunt, M.J. King, H. Scher, Phys. Rev. A 46 (1992) 7680.
[34] N.R. Tas, J.W. Berenschot, P. Mela, H.V. Jansen, M. Elwenspoek, A. van den Berg, Nano Lett. 2 (2002) 1031.
[35] D.A. Czaplewski, J. Kameoka, R. Mathers, G.W. Coates, H.G. Craighead, Appl. Phys. Lett. 83 (2003) 4836.
[36] C. Lee, E.H. Yang, N.V. Myung, T. George, Nano Lett. 3 (2003) 1339.
[37] J. Klein, E. Kumacheva, J. Chem. Phys. 108 (1998) 6996.